

# NOISY AERODYNAMIC RESPONSE AND SMOOTH APPROXIMATIONS IN HSCT DESIGN

Anthony A. Giunta\*, Jane M. Dudley\*, Robert Narducci\*,  
Bernard Grossman†, Raphael T. Haftka‡, William H. Mason§, and Layne T. Watson¶  
Multidisciplinary Analysis and Design Center for Advanced Vehicles  
Virginia Polytechnic Institute and State University  
Blacksburg, Virginia 24061-0203

## ABSTRACT

Convergence difficulties were encountered in our recent efforts toward a combined aerodynamic-structural optimization of the High Speed Civil Transport (HSCT). The underlying causes of the convergence problems were traced to numerical noise in the calculation of aerodynamic drag components for the aircraft. Two techniques were developed to circumvent the obstacles to convergence. The first technique employed a sequential approximate optimization method which used large initial move limits on the design variables. This helped dislodge the optimizer out of the local minima in the design space created by the noisy drag data. The second method utilized response surface methods to construct smooth approximations to the noisy data. The response surfaces were formed by analyzing several individual HSCT configurations and then fitting polynomial functions to selected objective function data. A simplified example design problem was used to demonstrate the response surface technique and to investigate various other issues relating to the construction of the response surfaces.

## 1. INTRODUCTION

The design of modern aerospace vehicles involves multidisciplinary interactions and presents a formidable challenge to the designer in a competitive marketplace. Multidisciplinary optimization (MDO) technology is a major tool for addressing this need, but its current use in the design process is limited by its enormous computational burden. To address this challenge, our group at

---

\* Graduate Research Assistant, Dept. of Aerospace and Ocean Engineering, Student Member AIAA

† Professor and Head, Dept. of Aerospace and Ocean Engineering, Associate Fellow AIAA

‡ Christopher C. Kraft Professor of Aerospace and Ocean Engineering, Associate Fellow AIAA

§ Associate Professor of Aerospace and Ocean Engineering, Associate Fellow AIAA

¶ Professor of Computer Science and Mathematics

Copyright © 1994 by American Institute of Aeronautics and Astronautics, Inc. All rights reserved.

Virginia Tech recently developed a variable-complexity modeling approach, involving the use of refined and computationally expensive models together with simple and computationally inexpensive models<sup>1</sup>. We have applied this approach to the combined aerodynamic-structural optimization of transport wings and recently have focused on the aerodynamic-structural optimization of the High Speed Civil Transport (HSCT)<sup>2-4</sup>.

The issues addressed in this paper arose in a recent HSCT study where we found that the final vehicle configurations varied significantly depending on the choice of initial conditions for the design variables. One of the causes of this problem was traced to numerical noise in the computation of aerodynamic drag components. This noise contributed to the formation of a jagged multidimensional objective function with many local minima. It appeared that our previous HSCT designs had become trapped in these local minima during the optimization process and were prevented from converging to an optimal configuration.

This paper describes two techniques for constructing smooth approximations to the drag components in an effort to counter the noisy, drag data. The first utilizes a variation on the sequential aerodynamic optimization techniques currently employed in our research. The second uses the concept of multipoint approximation and response surface methodology to replace the sequential evaluation of point designs. Response surface methods have been used by other investigators, *e.g.*, References 5 and 6.

## 2. DESIGN PROBLEM

### 2.1 HSCT Configuration

Successful aircraft configuration optimization requires a simple yet meaningful mathematical characterization of the geometry. We have developed a model that completely defines the wing-body-nacelle configuration, using twenty-six design variables. The wing planform is described by eight design variables, and the airfoil thickness distribution by an additional five. The nacelles move axially with the trailing-edge of the wing, and two parameters define their spanwise locations. The axisymmetric fuselage requires eight parameters

to specify both the axial positions and radii of the four fuselage restraint locations. Details of the geometry specification appear in References 4 and 7. While the configuration is defined using this set of parameters, the aircraft geometry is actually stored as a discrete numerical description in the Craidon format<sup>8</sup>.

## 2.2 HSCT Mission

The optimization problem is to minimize the take-off gross weight of an HSCT configuration with a range of 5500 nautical miles and a cruise speed of Mach 2.4 while transporting 251 passengers. For this mission, in addition to the geometric parameters mentioned above, three variables defined the idealized cruise mission. One variable was the mission fuel and the other two were the initial cruise altitude and the constant climb rate used in the range calculation. Fifty-five constraints which include performance/aerodynamic constraints and geometric constraints, such as fuselage volume and tail scrape angle, prevent the optimizer from creating physically improbable designs<sup>7</sup>.

## 3. SEQUENTIAL APPROXIMATE OPTIMIZATION

### 3.1 Variable-Complexity Modeling

Our detailed aerodynamic analysis utilized the Harris program<sup>9</sup> for the supersonic volumetric wave drag, a Mach-box<sup>10-12</sup> type method for supersonic drag due to lift, and a vortex-lattice program for landing performance. When compared to the computational costs of current computational fluid dynamics analysis techniques, the aerodynamic analysis methods used in this study are relatively inexpensive. However, when implemented in design optimization, where the same calculation may be repeated thousands of times, the cost associated with these techniques quickly becomes substantial. Therefore, we also employed simple, less computationally intensive analyses in a variable-complexity modeling approach<sup>2-4,7</sup>. We used this methodology within a sequential approximate optimization technique whereby the overall design process was composed of a sequence of optimization cycles. At the beginning of each cycle, approximations to the wave drag and drag due to lift were constructed using either linear, scaled, or global-local approximations<sup>2-4,7</sup>. The scaled approximation method was utilized in this study and employed a constant scaling function,  $\sigma$ , given as

$$\sigma(x_0) = \frac{f_d(x_0)}{f_s(x_0)}, \quad (1)$$

where  $f_d$  represents a detailed model analysis result, and  $f_s$  represents a simple model analysis result, both

evaluated at a specified design point,  $x_0$ , at the beginning of an optimization cycle. During an optimization cycle, the scaled approximate analysis results,  $f(x)$ , were calculated as

$$f(x) = \sigma(x_0)f_s(x). \quad (2)$$

Move limits then were imposed on the design variables to avoid large errors, and the optimization was performed using the NEWSUMT-A program<sup>13</sup>, which implements a sequential unconstrained minimization technique utilizing an extended interior penalty function. At the end of the optimization cycle the scaling function  $\sigma$  was recalculated and the above process was repeated.

### 3.2 Design Convergence Problems

In optimizing the HSCT, two kinds of convergence difficulties were encountered. First, at the completion of the final optimization cycle, there was little improvement in the objective function when compared to the objective function evaluated from the initial data. Second, when the optimization process was restarted using different initial design variables, it converged to different final HSCT configurations. This is demonstrated in Figure 1 which shows two different starting design planforms and the corresponding, unconverged final design planforms. The failure to converge to a single final design occurred because the optimizer was trapped in spurious local minima. Further, the optimization process was impeded by the inaccurate sensitivity derivatives stemming from the noisy analysis results.

### 3.3 Large Move Limit Method

During a standard optimization process the move limits on the variables initially were approximately eight percent and were decreased to approximately two percent as the optimization neared completion. In an attempt to prevent the optimizer from becoming trapped in spurious local minima, the move limits were increased to approximately thirty percent at the start of the optimization and then decreased as the optimization progressed. Error in the approximate analysis introduced through the use of large initial move limits was deemed acceptable because of the previous optimization difficulties. This technique previously was employed for a different problem by Joh, et al<sup>14</sup>. Through the use of these much larger move limits, the optimizer initially escaped from the local minima and proceeded to identify improved designs. However, the newly found improved designs did not converge to a single HSCT configuration as demonstrated by the planform views shown in Figure 1.

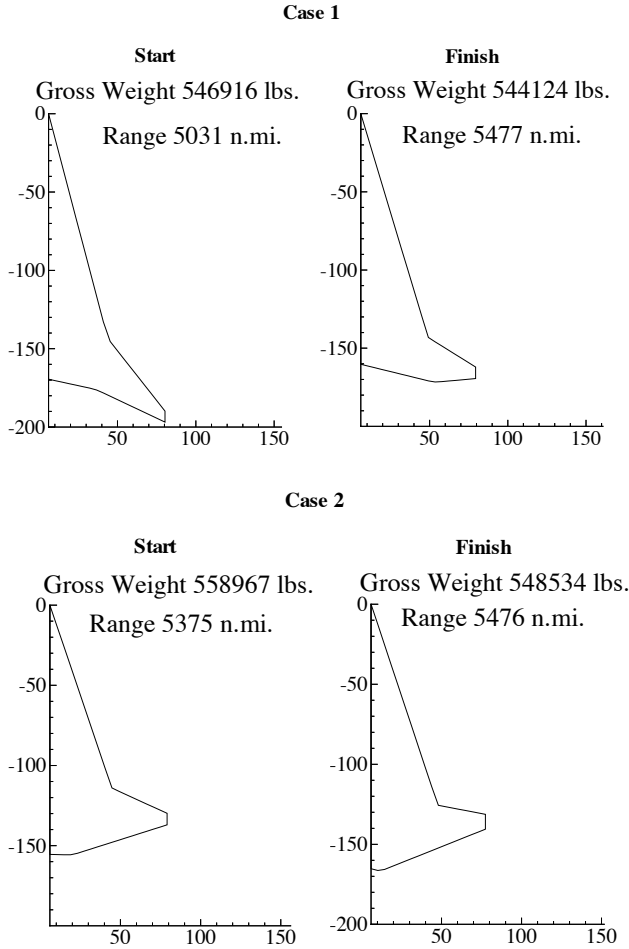


Figure 1. Dissimilar converged designs from different starting conditions due to spurious local minima. (All dimensions in feet.)

#### 4. NOISY DRAG CALCULATIONS

As described above, our current HSCT design optimization research involves up to twenty-six design variables and fifty-five constraints. Therefore, the optimization problem is to locate optimal HSCT configurations within a twenty-six dimensional design space defined by the limits of the design variables. To study difficulties associated with the optimization process, we selected an example design problem involving only two design variables. Thus, the three dimensional graph of the objective function may be easily visualized when plotted against the two design variables. In this example problem, the remaining twenty-four variables were held constant and the constraints were not applied to the HSCT configurations that were examined.

#### 5. TWO DESIGN VARIABLE PROBLEM

For the example problem, the two design variables were the axial locations for the leading-edge and

trailing-edge break points on the HSCT wing planform as shown in Figure 2. The design variables were varied by  $\pm$  ten percent from the current baseline HSCT configuration used in our studies. This corresponded to a variation of the inboard leading-edge sweep angle from  $77^\circ$  to  $79^\circ$  and a variation of the inboard trailing-edge sweep angle from  $-55^\circ$  to  $50^\circ$ . Figure 3 shows planform views of the four HSCT configurations defined by the limits of the design variables. Because the design constraints were not applied in the example problem, several of the HSCT configurations in Figure 3 are quite unrealistic. To investigate the noisy drag data, we selected the supersonic drag due to lift as the objective function.

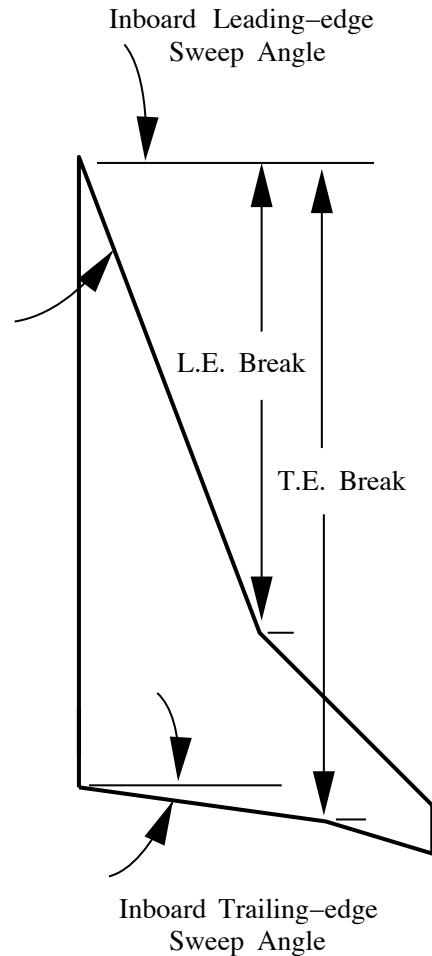
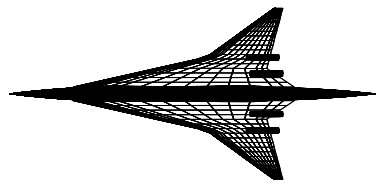


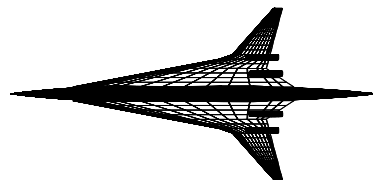
Figure 2. Design variable definition for the example problem.

The design space was then discretized using a  $21 \times 41$  uniform grid, and supersonic drag due to lift was calculated for the HSCT configuration at each point on the mesh. This produced a detailed map of the objective function, shown in Figure 4, where drag due to lift is plotted versus the range of leading and trailing-edge sweep angles. Figure 5 shows a cross sectional cut of the

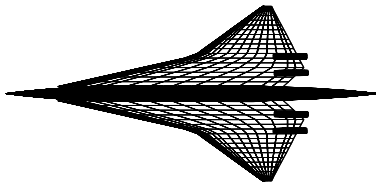
## HSCT Design Examples



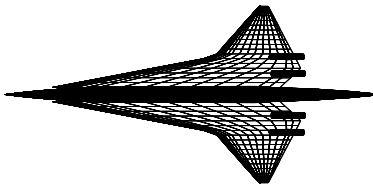
L.E. Sweep = 77 deg.  
T. E. Sweep = -55 deg.  
 $CD(lift)/CL^2 = 0.567$



L.E. Sweep = 79 deg.  
T. E. Sweep = -55 deg.  
 $CD(lift)/CL^2 = 0.569$



L.E. Sweep = 77 deg.  
T. E. Sweep = 50 deg.  
 $CD(lift)/CL^2 = 0.580$



L.E. Sweep = 79 deg.  
T. E. Sweep = 50 deg.  
 $CD(lift)/CL^2 = 0.573$

Figure 3. Extreme HSCT planforms obtained at the limits of the design space.

three dimensional surface taken at a trailing-edge angle of approximately three degrees. Note the extremely fine scale of the noise with respect to both the variation in sweep angle and in the drag due to lift values. This view of the drag demonstrates the jagged surface features which created the multiple spurious local minima. Similar results were obtained for the volumetric wave drag.

The irregular surface features shown in Figure 4 can be attributed to the techniques used in the supersonic drag due to lift calculations. The methods of Carlson et al.<sup>10-12</sup> utilize a paneling scheme that is sensitive to planform changes. Thus, slight modifications to the leading and trailing-edge sweep angles along with changes in the location where the Mach angle intersected the leading-edge, produced discontinuous variations in the predicted drag. The variations are small enough so that at all points the accuracy of the drag is acceptable. However, the oscillatory behavior creates difficulties for gradient based optimization techniques.

It is interesting to note that similar oscillatory behavior was encountered in a nozzle design problem<sup>15</sup> in which an Euler flow solver was employed. Thus, such oscillatory problems are not solely related to the use of panel method flow solvers.

## 6. RESPONSE SURFACE METHODS

Multipoint approximation methods provide an alternative approach to the sequential approximation techniques described above. The term *multipoint* refers to the practice of concurrently analyzing many different HSCT configurations; a process which is inherently amenable to parallel computing. The multipoint analyses yield a database containing both the independent design variables and objective function data. *Response surfaces* are smooth functions which define the relationship between the independent and dependent variables<sup>16</sup>.

The goal of multipoint approximation is to model either the objective function on the entire design space or portions of it using smooth response surfaces. Since the topography of a multidimensional objective function generally is unknown and may have many local minima, the smooth functions are selected so that the prominent features of the objective function are retained. Thus, in the optimization process, the region where the global minimum exists may be readily found while spurious local minima may be avoided.

This work focuses on the use of multipoint approximations to fit response surfaces to the noisy objective function of the example problem. Although the

drag due to lift calculations are noisy (Fig. 4), the variation in the drag is only 2.5 percent. Since the range of variation is small, low order response surfaces based on linear and quadratic functions can be used to model the topography of the objective function. In the present work response surface methodology has been applied using surfaces produced by bilinear tensor products, quadratic polynomials, biquadratic tensor products, and rational functions.

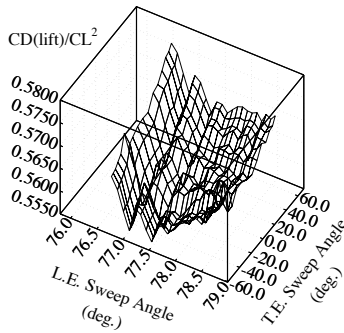


Figure 4. Noisy drag due to lift objective function data in the design space.

Because of the computational costs associated with evaluating the large number of point designs required for multipoint approximation, the present work focuses on methods to determine the minimum number of calculations required to construct various response surfaces. The simple models and the mathematical techniques developed for this work with two design variables will be extended later to design problems involving many variables where computational costs are significant.

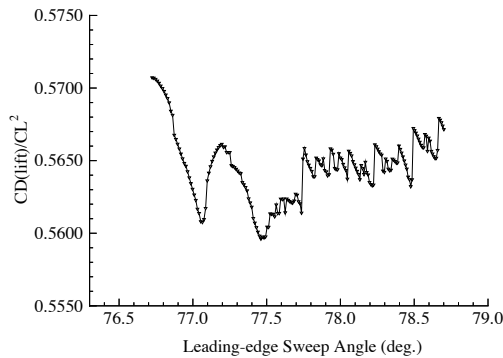


Figure 5. Drag due to lift vs. leading-edge sweep angle. Trailing-edge sweep angle approximately three degrees.

Response surface approximations to the surface in Figure 4 were constructed using both polynomial functions and rational functions. The bilinear tensor product model has the form

$$f(x, y) = (a_1x + a_2)(a_3y + a_4). \quad (3)$$

Also employed were the quadratic polynomial

$$f(x, y) = a_1x^2 + a_2xy + a_3x + a_4y^2 + a_5y + a_6 \quad (4)$$

and the biquadratic tensor product

$$f(x, y) = (a_1x^2 + a_2x + a_3)(a_4y^2 + a_5y + a_6). \quad (5)$$

In addition to these models, the (1,1) rational function

$$f(x, y) = \frac{a_1x + a_2y + a_3}{a_4x + a_5y + a_6} \quad (6)$$

was utilized.

The construction and evaluation of a response surface requires several steps. In the first step a number of points were selected using one of the point selection techniques discussed below. Supersonic drag due to lift data were then calculated at each of the design points and a response surface was fit to the data. For the bilinear tensor product, quadratic polynomial, and biquadratic tensor product the response surfaces were found by performing a linear least squares fit to the drag due to lift data. For the rational function approximation, a Levenberg-Marquardt nonlinear least squares fitting routine was used. For this problem, the residual was defined as the difference between the objective function values on the computed surface and corresponding model values on the response surface. From the residual data the average error, RMS error, and maximum error of the residual were calculated to evaluate the quality of the response surface fits.

## 7. POINT SELECTION TECHNIQUES

To construct a response surface for an objective function described by  $n$  independent variables, a large number of individual configuration analyses were required. To use computational resources wisely, the designer must consider both the quantity and the distribution of the design points in the  $n$ -dimensional design space. In this regard, we have examined three design point selection and distribution techniques:  $D$ -optimal, central composite design, and random. The validity of these depend on statistical assumptions about the nature of the drag noise. It may be that other statistical estimation procedures, such as robust M- or LMS-estimation, are more appropriate for the drag noise.

## 7.1 $D$ -Optimal Criterion

One method for selecting points to be used in response surface construction is to choose points in the design space which satisfy the  $D$ -optimal criterion. A discussion of this criterion is presented by Box and Draper<sup>17</sup>. To explain the  $D$ -optimal criterion, or  $D$ -optimality, we consider the linear system  $Y = \mathbf{X}c$ , where  $Y$  is the  $m$  by 1 vector of objective function values,  $c$  is the  $k$  by 1 vector of coefficients to be estimated, and  $\mathbf{X}$  is an  $m$  by  $k$  matrix of constants having rank  $k$ . The rows of matrix  $\mathbf{X}$  are formed from the response surface functions which relate the independent variables to the evaluated objective function at each design point. For example, in a two variable design space for which there are  $m$  objective function values and the response surface model is  $y = c_1 + c_2x_1 + c_3x_2$ , the system has the form

$$\begin{pmatrix} y(x_{1,1}, x_{2,1}) \\ y(x_{1,2}, x_{2,2}) \\ \vdots \\ y(x_{1,m}, x_{2,m}) \end{pmatrix} = \begin{pmatrix} 1 & x_{1,1} & x_{2,1} \\ 1 & x_{1,2} & x_{2,2} \\ \vdots & \vdots & \vdots \\ 1 & x_{1,m} & x_{2,m} \end{pmatrix} \begin{pmatrix} c_1 \\ c_2 \\ c_3 \end{pmatrix}. \quad (7)$$

From this system, the least squares estimate of  $c$  is  $\hat{c} = (\mathbf{X}^T \mathbf{X})^{-1} \mathbf{X}^T Y$ . To satisfy  $D$ -optimality we find the  $m$  points from a set of  $l > m$  candidate points existing in the design space that will yield the best fidelity between the polynomial model and the actual objective function. The  $D$ -optimality criterion states that the  $m$  points to choose are those which maximize the determinant  $|\mathbf{X}^T \mathbf{X}|$ . Several properties of this criterion are:

- i. the set of points that maximizes  $|\mathbf{X}^T \mathbf{X}|$  is also the set of points that minimizes the maximum variance of any predicted value of the objective function,
- ii. the set of points that maximizes  $|\mathbf{X}^T \mathbf{X}|$  is also the set of points that minimizes the variance of the parameter estimates,
- iii. the design obtained is invariant to changes in scale.

The problem of finding the  $m$  points that will give us the most loyal approximation is the problem of finding the  $m$  points that will maximize  $|\mathbf{X}^T \mathbf{X}|$ . We create a set of  $l > m$  points by forming a grid over the design space. Points of intersecting grid lines become candidate points. Conceivably, one could consider each of the  $\binom{l}{m} = l!/(m!(l-m)!)$  combinations of  $m$  points from the set of  $l$  candidate points, evaluate  $|\mathbf{X}^T \mathbf{X}|$ , and identify the set with the largest determinant. A small problem in two design variables may be to pick twenty-five points from 121 possible points (discretizing the design domain into ten sections in both directions leads to an  $11 \times 11$  mesh). This leads to a total of  $5.26 \cdot 10^{25}$  possible combinations, one or more of which are  $D$ -optimal.

It is clear that a heuristic method must be applied to estimate the optimum  $|\mathbf{X}^T \mathbf{X}|$ . This nonconvex combinatorial optimization problem is difficult because:

- i. the discrete feasible set is huge, and
- ii.  $|\mathbf{X}^T \mathbf{X}|$  may have local maxima.

For lack of a better alternative we use a genetic algorithm (GA) to maximize  $|\mathbf{X}^T \mathbf{X}|$ .

### 7.1.1 Genetic Algorithm to find $D$ -optimality

The GA employed here is roughly modeled after the algorithm described in the paper by Furuya and Haftka<sup>18</sup>. A general description of a GA follows. The GA works with a population of  $b$  designs, each representing a choice of  $m$  out of  $l$  possible points. The population of designs goes through a selection process for breeding, whereby designs with a higher merit function,  $|\mathbf{X}^T \mathbf{X}|$  here, have a higher probability of being selected for breeding. Breeding is performed in such a manner that the child designs maintain some likeness to the parent designs. The next generation of designs is comprised of  $b - 1$  children created during the breeding process plus the best parent design of the parent generation. Thus, the population size remains constant throughout the generations. This is known as an "elitist" strategy. The process continues for many generations, and terminates after a fixed number of generations, although there are many other reasonable stopping criteria which may be applied. The design with the best merit function in the end is used. The specifics of the GA as applied to seeking  $D$ -optimality are described in the following paragraphs.

The intent of the GA is to select the group of  $m$  points that satisfy  $D$ -optimality for the purpose of constructing a least squares approximation to the objective function. Any group of  $m$  distinct points among the  $l$  points is called a candidate. To start the algorithm, an initial population of  $b$  candidates is created. Each candidate is formed by randomly selecting  $m$  distinct points from the set of  $l$  points spanning the design space. A genetic string, made from the coordinates of the  $m$  points, is used to describe the candidate. For example, in a three dimensional design space, if  $m = 4$ , the genetic string of a particular design would be

$$x_{1,1} \ x_{2,1} \ x_{3,1} \ x_{1,2} \ x_{2,2} \ x_{3,2} \ x_{1,3} \ x_{2,3} \ x_{3,3} \ x_{1,4} \ x_{2,4} \ x_{3,4}.$$

The length  $G$  of the genetic string (the number of genes) is the dimension  $n$  of the design space multiplied by  $m$  ( $G = 12$  in the above example).

The candidates are selected as parents for breeding based on the fitness  $|\mathbf{X}^T \mathbf{X}|$ . Candidates with a higher fitness will be selected more often than candidates with lower fitness. The rank fitness is defined as  $b + 1 - r$ , where  $r$  is the rank of the candidate in the population in terms of the value of  $|\mathbf{X}^T \mathbf{X}|$ . The probability of selection as a parent is proportional to the rank fitness,

so that the probability of the  $r$ th ranked design being selected as a parent is

$$p_r = \frac{(b+1-r)}{b(b+1)/2}. \quad (8)$$

The selection process for parenting is completed by generating a uniformly distributed random number  $x$  between zero and one, and selecting the  $r$ th ranked design satisfying  $P_r \leq x < P_{r+1}$ , where

$$P_r = \sum_{i=1}^{r-1} p_i. \quad (9)$$

After two parents have been selected the breeding process begins. A random integer  $j$  between one and  $G-1$  (the number of genes-1) is generated. The child is constructed from the first  $j$  genes of the first parent and the  $G-j$  genes from the second parent. Note that this makes sense only if the design space is a Cartesian product. Otherwise, the new design may fall outside the design space. In that case, a much more complicated breeding scheme (“crossover” in GA parlance) or some penalty method would be necessary. Once the child is generated it goes through a mutation process. Each gene has a chance of mutating, and a fifteen percent chance was used in the present work. If a gene is selected for mutation, the gene is replaced with a gene coming randomly from the set of allowable values for that gene. Finally the child is checked for uniqueness and duplicate points. If it is a duplicate or has duplicate points, it is destroyed.

After  $b-1$  children are created, the parent generation is replaced, retaining only the best parent for the next generation. After the given number of generations have been created, the candidate with the highest  $|\mathbf{X}^T \mathbf{X}|$  is used for forming the response surface. There is no guarantee that the output of the genetic algorithm is truly  $D$ -optimal. However, known  $D$ -optimal sets of points for test cases have been recovered using the GA.

### 7.1.2 $D$ -Optimal Points in the Example

Our example problem required the selection of  $m$   $D$ -optimal points from the set of 861 drag due to lift data points which were used to construct Figure 4. The genetic algorithm described above was used to search through a portion of the  $861!/(m!(861-m)!)$  possible point combinations to estimate a  $D$ -optimal set of points. Once the best estimate of a set of  $D$ -optimal points was obtained, the appropriate response surface functions were fit to the data. Note that the GA was only used to choose the  $m$  point locations in the design space. The GA was not used to find the optimum HSCT configuration which minimized drag due to lift.

For the GA used in this problem, the population size for each generation was fixed at ten. The number of generations varied from 2000 to 25000 depending on

the number of points,  $m$ , needed for constructing the various response surfaces. The values for  $|\mathbf{X}^T \mathbf{X}|$  were monitored during the breeding process. When  $|\mathbf{X}^T \mathbf{X}|$  remained unchanged for approximately 1000 generations, the breeding process was terminated. As stated above, each gene had a fifteen percent chance of mutating during each generation.

Trailing-edge  
Sweep Angle (deg.)

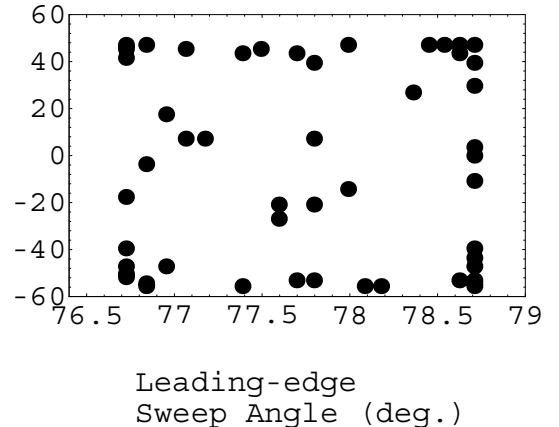


Figure 6. Fifty  $D$ -optimal design points chosen by GA for a quadratic response surface fit.

Figure 6 shows an example set of fifty points obtained by the GA for a quadratic polynomial response surface model. Note that the points lie predominately along on the perimeter of the design space. For a bilinear tensor product response surface model, all points lie on the perimeter. This behavior is expected since points near the perimeter of the design space have the strongest influence on  $|\mathbf{X}^T \mathbf{X}|$ .

## 7.2 Central Composite Design Criteria

A second candidate point selection criterion is called central composite design (CCD). This criterion, which is based on design of experiments theory<sup>19</sup>, permits the evaluation of both the quadratic and linear terms in equations (3-6) using a total of  $2^n + 2n + 1$  points, where  $n$  is the number of design variables. This is in contrast to the  $3^n$  points required for a full factorial design. For  $n$  greater than two, the set of CCD points is smaller than the set of  $3^n$  points. Unfortunately, for twenty-six design variables, even CCD requires an unacceptably large number of evaluations. However, the CCD criterion provides a useful standard of comparison to the other point selection techniques.

For the example problem where  $n = 2$ , the CCD method requires nine point analyses, which is the same as that required for a  $3^n$  full factorial design. However,

the location of the CCD points in the design space is different than the location of the full factorial points as shown in Figure 7, where the parameter  $\beta = (2^n)^{1/4}$  determined the spacing for the CCD points. Supersonic drag due to lift data were calculated for the CCD points and the response surfaces were fit to the objective function data.

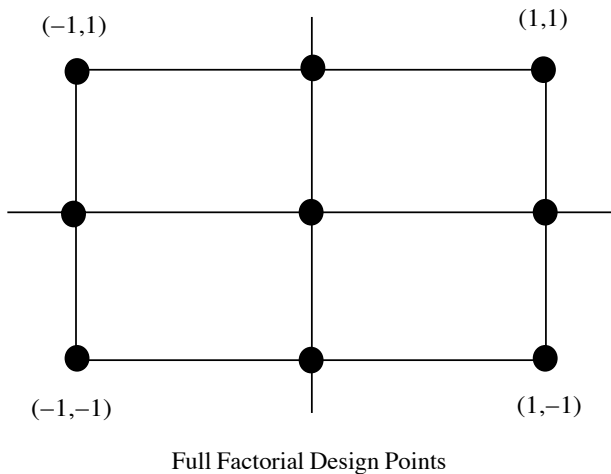
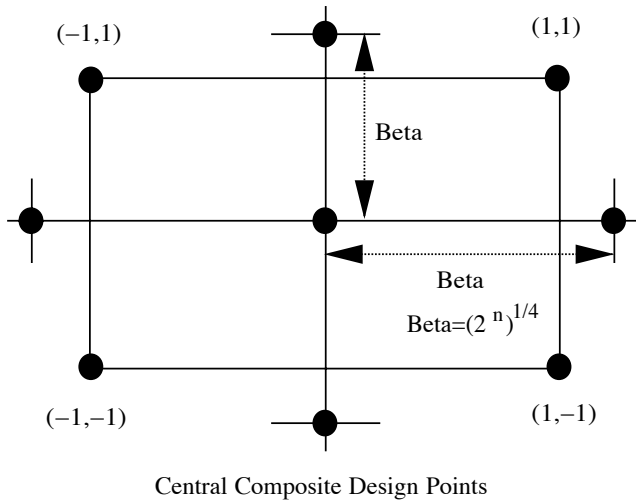


Figure 7. CCD and full factorial design point distributions for a two variable problem.

### 7.3 Random Point Selection

In this point selection technique  $m$  unique points were randomly chosen from the set of 861 drag due to lift data points used to construct Figure 4. For this process a uniform random integer generator, with a range from one to 861, was used. If duplicate points were selected, the repeated points were replaced by new randomly chosen points until all  $m$  points were unique.

Trailing-edge  
Sweep Angle (deg.)

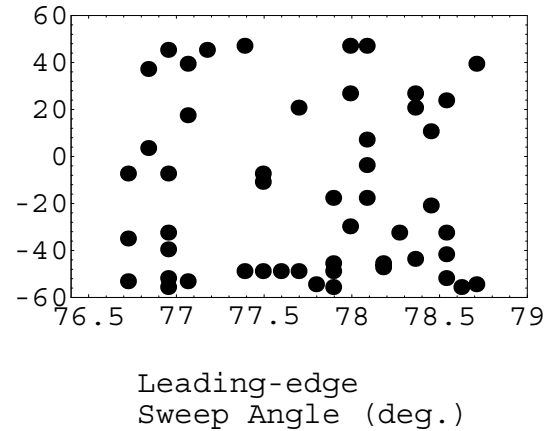


Figure 8. Fifty randomly chosen design points for a quadratic response surface fit.

Figure 8 shows an example distribution of fifty, unique, randomly selected points. Note the difference in the point distribution between the  $D$ -optimal set of points, the CCD points, and the randomly selected points.

## 8. RESULTS

Example response surfaces generated using equations (3-5) are shown in Figures 9a,b,c, respectively. These figures were generated using 100 randomly selected points in the design space, which was well above the minimum number of points needed to construct a response surface which adequately modeled the objective function. We discovered initially that the rational function described by equation (6) produced response surfaces similar to those of the bilinear tensor product. Therefore, further analysis using the rational function was not conducted.

Although the bilinear response surface provides a reasonable prediction of the overall trend of the computed noisy surface in Figure 4, it is evident that the quadratic and biquadratic response surfaces best capture the trends of the noisy surface. In particular, the global minimum on the noisy surface occurs for a leading-edge sweep angle of approximately  $75.6^\circ$  and a trailing-edge sweep angle of approximately  $-20.0^\circ$ , which is roughly predicted in Figures 9b,c.



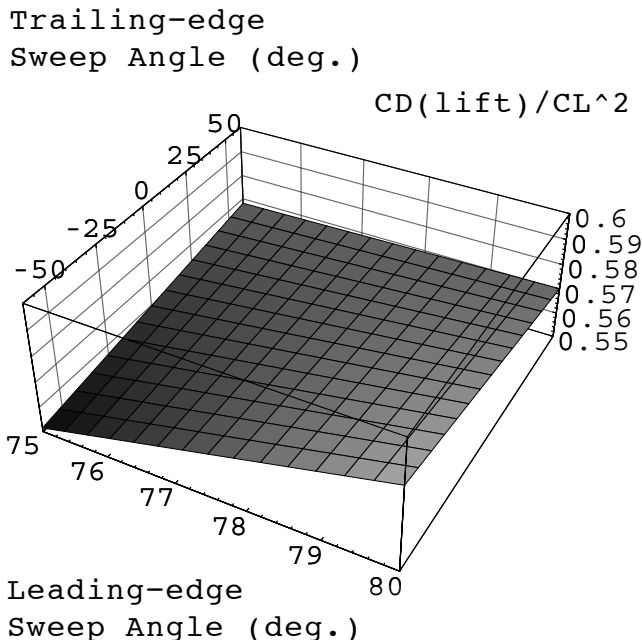


Figure 9a. Example bilinear tensor product response surface fit to the noisy objective function data.

The average error, RMS error, and maximum error of the residuals for each of the response surface functions and point selection techniques are listed in Tables 1-3. For the randomly selected data the values shown are averages for either three or five trials as indicated under each column. Data for the  $D$ -optimal and CCD data are for single trials only. Note that the results for  $m = 4, 6,$  and  $9$  points represent the minimum number of points needed to construct the bilinear, quadratic, and biquadratic response surfaces, respectively.

The errors associated with the bilinear tensor product response surfaces are given in Table 1 and show that the error for the  $D$ -optimal points decreased only slightly as the number of points ranged from four to twenty. This was to be expected since the  $D$ -optimality criteria specified points on the perimeter of the design space when bilinear response surface functions were used to form  $\mathbf{X}$  in equation (7). Thus, the points on the perimeter were effective in capturing the overall trend of the noisy surface, but adding additional points on the perimeter did little to change the overall quality of the fit. In contrast to the  $D$ -optimal error, the error for the randomly selected data points decreased considerably as  $m$  increased. This trend also was expected since response surfaces constructed using points mainly in the interior of the design space were more likely to be affected by the noise in the computed data. As the number of randomly selected points increased, the effects of the noise were canceled out and the surface fits

improved. This explains why the error for the randomly selected points was lower than the errors for the  $D$ -optimal points when more than ten points were used to construct the response surfaces. The error calculations for the nine CCD points were approximately the same as those for the randomly selected points and are somewhat better than for the  $D$ -optimal points. For the relatively simple bilinear tensor product model, all three point selection techniques provide point distributions which result in sufficiently accurate response surfaces comparable to that shown in Figure 9a.

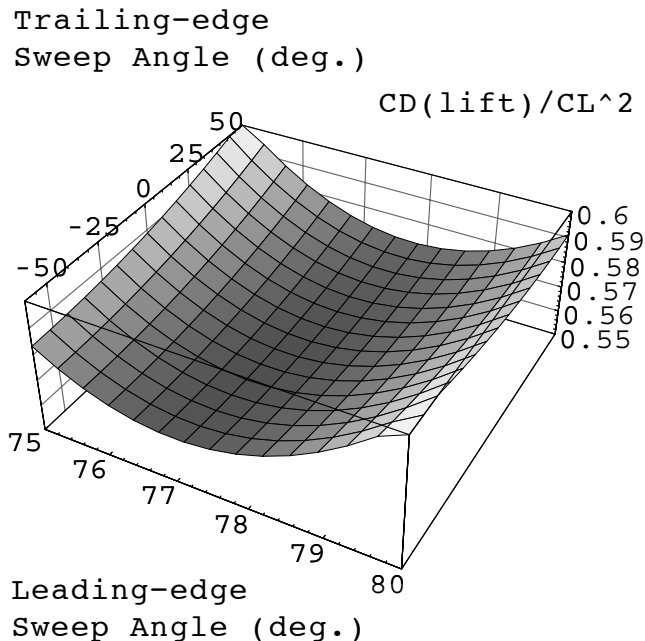


Figure 9b. Example quadratic polynomial response surface fit to the noisy objective function data.

Similar trends for the  $D$ -optimal and random points again occur in the error for the quadratic polynomial response surface as  $m$  increased from six to fifty points (Table 2). However, the error achieved using ten  $D$ -optimal points provided the same level of accuracy as was attained using approximately twenty to thirty randomly selected points. Further, all response surfaces produced from the  $D$ -optimal points were similar to the quadratic response surface shown in Figure 9b. In contrast, the response surfaces produced by the randomly selected points were significantly different than Figure 9b until at least twenty randomly selected points were used. The error from the response surface fit for the CCD points again was comparable to that of the  $D$ -optimal and randomly selected points. For the quadratic polynomial response surface the  $D$ -optimal and CCD points required fewer points to accurately model the noisy surface and therefore are superior to the random selection of points.

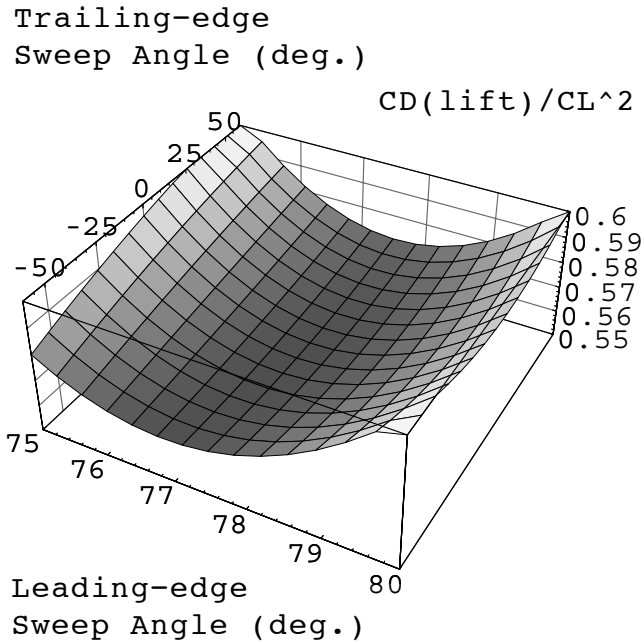


Figure 9c. Example biquadratic tensor product response surface fit to the noisy objective function data.

$m$	Avg. Error	RMS Error	Max. Error
D-optimal Points			
4	0.00413	0.00502	0.01490
5	0.00403	0.00492	0.01468
10	0.00381	0.00470	0.01416
15	0.00409	0.00496	0.01502
20	0.00378	0.00464	0.01414
Random Points*			
4	0.06568	0.09958	0.34724
5	0.00506	0.00685	0.02310
10	0.00278	0.00355	0.01171
15	0.00260	0.00339	0.01171
20	0.00268	0.00347	0.01222
CCD Points			
9	0.00587	0.00662	0.01579

Table 1. Calculated error for the bilinear tensor product response surface fit.

\*Average of three trials for each value of  $m$ .

$m$	Avg. Error	RMS Error	Max. Error
D-optimal Points			
6	0.00189	0.00247	0.00933
10	0.00215	0.00284	0.01102
20	0.00192	0.00252	0.01034
30	0.00192	0.00234	0.00855
40	0.00193	0.00244	0.00892
50	0.00211	0.00258	0.00779
Random Points*			
6	0.02178	0.03308	0.10160
10	0.00270	0.00357	0.01198
20	0.00227	0.00283	0.00906
30	0.00197	0.00251	0.00925
40	0.00193	0.00247	0.00906
50	0.00191	0.00240	0.00881
CCD Points			
9	0.00270	0.00331	0.00972

Table 2. Calculated error for the quadratic polynomial response surface fit.

\*Average of five trials for each value of  $m$ .

The error for the biquadratic tensor product response surfaces is shown in Table 3 for the three point selection techniques. As demonstrated with the previous response surface functions, the error for the  $D$ -optimal points varied little as  $m$  increased and the response surfaces were qualitatively in good agreement with Figure 9c. Approximately fifty randomly selected points were required to provide the same quality of fit as did ten  $D$ -optimal points. This further demonstrates that random point selection is not an efficient point selection method for response surface formation. The CCD points provide a quality of fit that is somewhat less accurate than the  $D$ -optimal points, but the response surface formed using the CCD points did not qualitatively agree well with Figure 9c. For the biquadratic tensor product, the  $D$ -optimal points provided the most accurate fit to the noisy surface, while the CCD points provided an adequate fit as well. The random point selection technique clearly is least acceptable due to the large number of points necessary to fit the noisy surface accurately.

$m$	Avg. Error	RMS Error	Max. Error
D-optimal Points			
9	0.00199	0.00259	0.01044
10	0.00201	0.00263	0.00996
20	0.00202	0.00251	0.00774
30	0.00199	0.00240	0.00810
40	0.00183	0.00232	0.00823
50	0.00184	0.00233	0.00893
60	0.00189	0.00234	0.00782
70	0.00188	0.00240	0.00875
80	0.00182	0.00231	0.00907
90	0.00181	0.00231	0.00900
100	0.00180	0.00226	0.00855
Random Points*			
9	0.04653	0.08443	0.51657
10	0.01706	0.02994	0.14234
20	0.00300	0.00414	0.01657
30	0.00251	0.00363	0.01793
40	0.00219	0.00292	0.01172
50	0.00200	0.00253	0.00995
60	0.00193	0.00241	0.00869
70	0.00192	0.00244	0.00868
80	0.00185	0.00234	0.00878
90	0.00184	0.00231	0.00889
100	0.00186	0.00231	0.00845
CCD Points			
9	0.00310	0.00399	0.01262

Table 3. Calculated error for the biquadratic tensor product response surface fit.

\*Average of five trials for each value of  $m$ .

## 9. FUTURE RESEARCH DIRECTIONS

For future research, several other areas of interest have been identified which will work in conjunction with the multipoint response surface methods we have developed thus far. To combat the “*curse of dimensionality*” which greatly increases the number of required point analyses as the dimension of the design space becomes large, we propose several avenues of investigation. First, we will apply the fifty-five constraints of our HSCT design problem to reduce the design space from an  $n$ -dimensional rectangle to a smaller  $n$ -dimensional feasible region in which we will concentrate our analysis points. The domain of design variables will be further reduced by only considering design variables in a vicinity of those found on the basis of a simple model analysis and optimization. This variable-complexity approach will play a large role in reducing the computational cost of the HSCT design problem. In addition, we plan to apply principal factor analysis

to identify which design variables have the most impact on the overall HSCT design. Those variables having the most effect will be modeled using higher order response surface functions while those having less effect will be modeled using lower order functions. Along with these efforts, we have started the process of converting the HSCT analysis codes to run on a parallel computer. Because the multipoint response surface methodology requires numerous independent calculations, it offers an excellent way to exploit coarse grained parallel computations and thereby reduce computational costs.

## 10. CONCLUDING REMARKS

In the optimization of the high speed civil transport the computed objective function was found to be extremely noisy, with many local minima. This noise inhibited the use of traditional gradient based sequential approximate optimization techniques because HSCT designs became trapped in spurious noise-induced local minima. A method of escaping these minima was found by using large move limits for the first few optimization cycles and then decreasing the move limits to reasonable sizes as the optimization progressed. This technique enabled the optimizer to escape local minima early in the optimization process and several improved designs were identified with this technique. However, no single, optimal HSCT configuration was achieved with this method.

As demonstrated in the two variable example problem, the use of response surface methodology provides a technique for calculating smooth approximations to noisy objective function data. The comparison between the three point selection techniques demonstrated that an ordered point selection technique, such as  $D$ -optimality or central composite design, provides a more accurate and efficient method of modeling the objective function than does random point selection. For the example problem where only two design variables were utilized, there was little difference between the  $D$ -optimal and CCD selection methods. However, for design problems involving more than two design variables, the number of analyses required for the CCD method quickly becomes infeasible. The  $D$ -optimal point selection technique provides a flexible approach for choosing analysis points within an  $n$ -dimensional design space and can be tailored to provide an optimum arrangement of any number of analysis points which the designer can computationally afford. Further, the use of a genetic algorithm has been shown to be a practical means of estimating a  $D$ -optimal set of analysis points.

## ACKNOWLEDGMENTS

This research was partially supported by NASA Grant NAG1-1160 with Mr. P. Coen as contract monitor and NASA Grant NAG1-1562, with Dr. P. Newman as contract monitor.

## REFERENCES

1. Unger, E. R., Hutchison, M. G., Rais-Rohani, M., Haftka, R. T., and Grossman, B., "Variable-Complexity Design of a Transport Wing," *Intl. J. Systems Automation: Res. and Appl. (SARA)*, No. 2, 1992, pp. 87–113.
2. Hutchison, M. G., Huang, X.-M., Mason, W. H., Haftka, R. T., and Grossman, B., "Variable-Complexity Aerodynamic-Structural Design of a High-Speed Civil Transport Wing," AIAA Paper 92-4695, Sept. 1992.
3. Hutchison, M. G., Unger, E. R., Mason, W. H., Grossman, B., and Haftka, R. T., "Variable-Complexity Aerodynamic Optimization of an HSCT Wing Using Structural Wing-Weight Equations," *J. Aircraft*, vol. 31, No. 1, 1994, pp. 110–116.
4. Hutchison, M. G., Unger, E. R., Mason, W. H., Grossman, B., and Haftka, R. T., "Aerodynamic Optimization of an HSCT Wing Using Variable-Complexity Modeling," AIAA Paper 93-0101, Jan. 1993.
5. Healy, M. J., Kowalik, J. S., and Ransay, J. W., "Airplane Engine Selection by Optimization on Surface Fit Approximations," *J. Aircraft*, vol. 12, No. 7, 1975, pp. 593–599.
6. Englund, W. C., Stanley, D. O., Lepsch, R. A., McMillian, M. M., and Unal, R., "Aerodynamic Configuration Design Using Response Surface Methodology Analysis," AIAA Paper 93-3967, Aug. 1993.
7. Hutchison, M. G., "Multidisciplinary Optimization of High-Speed Civil Transport Configurations Using Variable-Complexity Modeling," Ph.D. Dissertation, VPI&SU, March 1993.
8. Craidon, C. B., "Description of a Digital Computer Program for Airplane Configuration Plots," NASA TM X-2074, 1970.
9. Harris, R. V., Jr., "An Analysis and Correlation of Aircraft Wave Drag," NASA TM X-947, 1964.
10. Carlson, H. W., and Miller, D. S., "Numerical Methods for the Design and Analysis of Wings at Supersonic Speeds," NASA TN D-7713, 1974.
11. Carlson, H. W., and Mack, R. J., "Estimation of Leading-Edge Thrust for Supersonic Wings of Arbitrary Planforms," NASA TP-1270, 1978.
12. Carlson, H. W., Mack, R. J., and Barger, R. L., "Estimation of Attainable Leading-Edge Thrust for Wings at Subsonic and Supersonic Speeds," NASA TP-1500, 1979.
13. Grandhi, R. V., Thareja, R., and Haftka, R. T., "NEWSUMT-A: A General Purpose Program for Constrained Optimization Using Constraint Approximation," *ASME J. Mechanisms, Transmissions and Automation in Design*, vol. 107, 1985, pp. 94–99.
14. Joh, C.-Y., Grossman, B., and Haftka, R. T., "Design Optimization of Transonic Airfoils," *Eng. Opt.*, vol. 21, No. 1, 1993, pp. 1–20.
15. Narducci, R., Grossman, B., and Haftka, R. T., "Sensitivity Algorithms for an Inverse Design Problem Involving a Shock Wave," AIAA Paper 94-0096, Jan. 1994.
16. Khuri, A. I., and Cornell, J. A., *Response Surfaces: Designs and Analyses*, Marcel Dekker, Inc., New York, N. Y., 1987.
17. Box, M. J. and Draper, N. R., "Factorial Designs, the  $|\mathbf{X}^T \mathbf{X}|$  Criterion, and Some Related Matters," *Technometrics*, vol. 13, No. 4, 1971, pp. 731–742.
18. Furuya, H. and Haftka, R. T., "Locating Actuators for Vibration Suppression on Space Trusses by Genetic Algorithms," ASME Winter Annual Meeting, 1993.
19. Mason, R. L., Gunst, R. F., and Hess, J. L., *Statistical Design and Analysis of Experiments*, John Wiley & Sons, New York, N. Y., 1989, pp. 215–221.